NASA Contractor Report 185154

Multigrid Calculations of 3-D Turbulent Viscous Flows

Jeffrey W. Yokota
Sverdrup Technology, Inc.
NASA Lewis Research Center Group
Cleveland, Ohio

October 1989

Prepared for
Lewis Research Center
Under Contract NAS3-25266

National Aeronautics and
Space Administration

Multigrid Calculations of 3-D Turbulent Viscous Flows

Jeffrey W. Yokota
Sverdrup Technology, Inc.
NASA Lewis Research Center Group
Cleveland, Ohio

Abstract

Convergence properties of a multigrid algorithm, developed to calculate compressible viscous flows, are analysed by a vector sequence eigenvalue estimate. The full three-dimensional Reynolds-averaged Navier-Stokes equations are integrated by an implicit multigrid scheme while a $k-\varepsilon$ turbulence model is solved, uncoupled from the flow equations. Estimates of the eigenvalue structure for both single and multigrid calculations are compared in an attempt to analyse the process as well as the results of the multigrid technique. The flow through an annular turbine is used to illustrate the scheme's ability to calculate complex three-dimensional flows.

Introduction

In many ways the use of computational fluid dynamics has been legitimised by the successful calculation of two-dimensional inviscid transonic flows. However, for computational fluid dynamics to have a continued impact on the aerodynamic design process, efficient three-dimensional methods must be developed. Because the greatest aerodynamic gains are now being realised by truly three-dimensional designs, the need to compute three-dimensional compressible viscous flows is apparent.

The present work deals with the analysis of a multigrid scheme to solve the Reynolds-averaged Navier-Stokes equations. The flow equations are solved by the diagonally inverted LU implicit multigrid scheme,[1] while the Reynolds stess tensor is modelled by a Boussinesq eddy-viscosity formulation which calculates turbulent viscosities from a high Reynolds number $k-\varepsilon$ model.

The multigrid method has been, by far, the most successful means of accelerating inviscid calculations to steady state. A number of researchers have recently extended this technique to viscous flow calculations. Although it is true that relatively greater benefits are produced with the Euler equations, a significant amount of acceleration is also produced with the Navier-Stokes equations. In an attempt to understand the process by which the multigrid method produces this acceleration, eigenvalue estimates are compared for both single and multigrid calculations of inviscid and viscous flows.

Analysis

The three-dimensional Reynolds-averaged Navier-Stokes equations, with the Boussinesq eddy-viscosity formulation, can be written in divergence form and then transformed from the Cartesian coordinate system (x,y,z) to the generalized system (ξ,η,ς). The Jacobians of the coordinate transformation are defined as

$$J=\begin{pmatrix} x_\xi & x_\eta & x_\varsigma \\ y_\xi & y_\eta & y_\varsigma \\ z_\xi & z_\eta & z_\varsigma \end{pmatrix} \qquad J^{-1}=\begin{pmatrix} \xi_x & \xi_y & \xi_z \\ \eta_x & \eta_y & \eta_z \\ \varsigma_x & \varsigma_y & \varsigma_z \end{pmatrix}=\frac{1}{D}\begin{pmatrix} y_\eta z_\varsigma - y_\varsigma z_\eta & x_\varsigma z_\eta - x_\eta z_\varsigma & x_\eta y_\varsigma - x_\varsigma y_\eta \\ y_\varsigma z_\xi - y_\xi z_\varsigma & x_\xi z_\varsigma - x_\varsigma z_\xi & x_\varsigma y_\xi - x_\xi y_\varsigma \\ y_\xi z_\eta - y_\eta z_\xi & x_\eta z_\xi - x_\xi z_\eta & x_\xi y_\eta - x_\eta y_\xi \end{pmatrix}$$

where D is the determinant of the matrix J. Contravariant velocity components $(U,V,W)^T=J^{-1}(u,v,w)^T$ can be derived from the Cartesian components (u,v,w) and then used in the transformed equations:

$$\frac{\partial \vec{W}}{\partial t}+\frac{\partial \vec{F}}{\partial \xi}+\frac{\partial \vec{G}}{\partial \eta}+\frac{\partial \vec{H}}{\partial \varsigma}=\frac{\partial \vec{F}_v}{\partial \xi}+\frac{\partial \vec{G}_v}{\partial \eta}+\frac{\partial \vec{H}_v}{\partial \varsigma} \tag{1}$$

with

$$\vec{W} = \begin{pmatrix} \rho D \\ \rho Du \\ \rho Dv \\ \rho Dw \\ \rho DE \end{pmatrix} \qquad \vec{F} = \begin{pmatrix} \rho DU \\ \rho DUu + PD\xi_x \\ \rho DUv + PD\xi_y \\ \rho DUw + PD\xi_z \\ DU(E+P) \end{pmatrix} \qquad \vec{G} = \begin{pmatrix} \rho DV \\ \rho DVu + PD\eta_x \\ \rho DVv + PD\eta_y \\ \rho DVw + PD\eta_z \\ DV(E+P) \end{pmatrix} \qquad \vec{H} = \begin{pmatrix} \rho DW \\ \rho DWu + PD\zeta_x \\ \rho DWv + PD\zeta_y \\ \rho DWw + PD\zeta_z \\ DW(E+P) \end{pmatrix}$$

$$\vec{F}_v = \begin{pmatrix} f_{v_1} \\ f_{v_2} \\ f_{v_3} \\ f_{v_4} \\ f_{v_5} \end{pmatrix} = \begin{pmatrix} 0 \\ D\xi_x\tau_{xx} + D\xi_y\tau_{xy} + D\xi_z\tau_{xz} \\ D\xi_x\tau_{xy} + D\xi_y\tau_{yy} + D\xi_z\tau_{yz} \\ D\xi_x\tau_{xz} + D\xi_y\tau_{yz} + D\xi_z\tau_{zz} \\ uf_{v_2} + vf_{v_3} + wf_{v_4} + \frac{\gamma}{\gamma-1}\tilde{\mu}_e(c_1\frac{\partial T}{\partial \xi} + c_2\frac{\partial T}{\partial \eta} + c_3\frac{\partial T}{\partial \zeta}) \end{pmatrix}$$

$$\vec{G}_v = \begin{pmatrix} g_{v_1} \\ g_{v_2} \\ g_{v_3} \\ g_{v_4} \\ g_{v_5} \end{pmatrix} = \begin{pmatrix} 0 \\ D\eta_x\tau_{xx} + D\eta_y\tau_{xy} + D\eta_z\tau_{xz} \\ D\eta_x\tau_{xy} + D\eta_y\tau_{yy} + D\eta_z\tau_{yz} \\ D\eta_x\tau_{xz} + D\eta_y\tau_{yz} + D\eta_z\tau_{zz} \\ ug_{v_2} + vg_{v_3} + wg_{v_4} + \frac{\gamma}{\gamma-1}\tilde{\mu}_e(c_4\frac{\partial T}{\partial \xi} + c_5\frac{\partial T}{\partial \eta} + c_6\frac{\partial T}{\partial \zeta}) \end{pmatrix}$$

$$\vec{H}_v = \begin{pmatrix} h_{v_1} \\ h_{v_2} \\ h_{v_3} \\ h_{v_4} \\ h_{v_5} \end{pmatrix} = \begin{pmatrix} 0 \\ D\zeta_x\tau_{xx} + D\zeta_y\tau_{xy} + D\zeta_z\tau_{xz} \\ D\zeta_x\tau_{xy} + D\zeta_y\tau_{yy} + D\zeta_z\tau_{yz} \\ D\zeta_x\tau_{xz} + D\zeta_y\tau_{yz} + D\zeta_z\tau_{zz} \\ uh_{v_2} + vh_{v_3} + wh_{v_4} + \frac{\gamma}{\gamma-1}\tilde{\mu}_e(c_7\frac{\partial T}{\partial \xi} + c_8\frac{\partial T}{\partial \eta} + c_9\frac{\partial T}{\partial \zeta}) \end{pmatrix}$$

where

$$\begin{aligned} c_1 &= D(\xi_x^2 + \xi_y^2 + \xi_z^2) \\ c_2 &= D(\xi_x\eta_x + \xi_y\eta_y + \xi_z\eta_z) \\ c_3 &= D(\xi_x\zeta_x + \xi_y\zeta_y + \xi_z\zeta_z) \\ c_4 &= D(\xi_x\eta_x + \xi_y\eta_y + \xi_z\eta_z) \\ c_5 &= D(\eta_x^2 + \eta_y^2 + \eta_z^2) \\ c_6 &= D(\eta_x\zeta_x + \eta_y\zeta_y + \eta_z\zeta_z) \\ c_7 &= D(\xi_x\zeta_x + \xi_y\zeta_y + \xi_z\zeta_z) \\ c_8 &= D(\eta_x\zeta_x + \eta_y\zeta_y + \eta_z\zeta_z) \\ c_9 &= D(\zeta_x^2 + \zeta_y^2 + \zeta_z^2) \end{aligned}$$

$$\begin{aligned} \tau_{xx} &= \tfrac{2}{3}\tilde{\mu}(2\tfrac{\partial u}{\partial x} - \tfrac{\partial v}{\partial y} - \tfrac{\partial w}{\partial z}) \\ \tau_{xy} &= \tilde{\mu}(\tfrac{\partial u}{\partial y} + \tfrac{\partial v}{\partial x}) \\ \tau_{xz} &= \tilde{\mu}(\tfrac{\partial u}{\partial z} + \tfrac{\partial w}{\partial x}) \\ \tau_{yy} &= \tfrac{2}{3}\tilde{\mu}(2\tfrac{\partial v}{\partial y} - \tfrac{\partial u}{\partial x} - \tfrac{\partial w}{\partial z}) \\ \tau_{yz} &= \tilde{\mu}(\tfrac{\partial v}{\partial z} + \tfrac{\partial w}{\partial y}) \\ \tau_{zz} &= \tfrac{2}{3}\tilde{\mu}(2\tfrac{\partial w}{\partial z} - \tfrac{\partial u}{\partial x} - \tfrac{\partial v}{\partial y}) \\ \\ \tilde{\mu} &= \mu_l + \mu_t \\ \tilde{\mu}_e &= \mu_l/Pr_l + \mu_t/Pr_t \end{aligned}$$

and ρ, P, and T are the fluid density, pressure, and temperature; and E is the total energy per unit volume. $Pr_l = 0.72$ is the laminar Prandtl number, $Pr_t = 0.90$ is the turbulent Prandtl number, μ_l is the laminar viscosity found from Sutherland's law, and μ_t is the turbulent viscosity obtained from the $k-\varepsilon$ turbulence model. The total energy and pressure of a calorically perfect gas are related through the equation of state $P = (\gamma - 1)(E - \rho\vec{v}\cdot\vec{v}/2)$, where $\gamma = 1.4$ is the ratio of specific heat capacities.

The eddy viscosity, μ_t, is modelled as:

$$\mu_t = C_\mu \frac{k^2}{\varepsilon} \tag{2}$$

where k, the turbulence kinetic energy, and ε, the dissipation rate of the turbulence kinetic energy, are obtained from the Launder and Spalding[2] high Reynolds number $k-\varepsilon$ turbulence model. C_μ is a scalar constant for isotropic turbulence and a wall function is used near solid boundaries. The $k-\varepsilon$ model has a number of benefits over the more widely used algebraic models. An explicit wake model is not required. This means that wakes do not have to be located and treated uniquely and are thus more likely to evolve and convect in a more realistic fashion. The wall function eliminates the need to sample information in a direction normal to solid boundaries thus making the calculation less sensitive to skewed or nonorthogonal mesh cells near solid walls. Furthermore this treatment, which makes no attempt to resolve the flow within the laminar viscous sublayer, requires fewer mesh cells and is thus less likely to be affected by the computational stiffness associated with highly stretched grids. Although it is true that heat transfer effects may not be modelled

accurately by a wall function, the stiffness of a low Reynolds number formulation and its corresponding poor convergence properties, are not present in the high Reynolds number model. The high Reynolds number $k-\varepsilon$ equations can be written:

$$\frac{\partial \vec{W}_{k\varepsilon}}{\partial t}+\frac{\partial \vec{F}_{k\varepsilon}}{\partial \xi}+\frac{\partial \vec{G}_{k\varepsilon}}{\partial \eta}+\frac{\partial \vec{H}_{k\varepsilon}}{\partial \zeta}=\vec{S}_{k\varepsilon} \tag{3}$$

where

$$\vec{W}_{k\varepsilon}=\begin{pmatrix}\rho Dk\\ \rho D\varepsilon\end{pmatrix} \qquad \vec{S}_{k\varepsilon}=\begin{pmatrix}s_1\\ s_2\end{pmatrix} \qquad \vec{F}_{k\varepsilon}=\begin{pmatrix}\rho DUk-\mu_k\left(c_1\frac{\partial k}{\partial \xi}+c_2\frac{\partial k}{\partial \eta}+c_3\frac{\partial k}{\partial \zeta}\right)\\ \rho DU\varepsilon-\mu_\varepsilon\left(c_1\frac{\partial \varepsilon}{\partial \xi}+c_2\frac{\partial \varepsilon}{\partial \eta}+c_3\frac{\partial \varepsilon}{\partial \zeta}\right)\end{pmatrix}$$

$$\vec{G}_{k\varepsilon}=\begin{pmatrix}\rho DVk-\mu_k\left(c_4\frac{\partial k}{\partial \xi}+c_5\frac{\partial k}{\partial \eta}+c_6\frac{\partial k}{\partial \zeta}\right)\\ \rho DV\varepsilon-\mu_\varepsilon\left(c_4\frac{\partial \varepsilon}{\partial \xi}+c_5\frac{\partial \varepsilon}{\partial \eta}+c_6\frac{\partial \varepsilon}{\partial \zeta}\right)\end{pmatrix} \qquad \vec{H}_{k\varepsilon}=\begin{pmatrix}\rho DWk-\mu_k\left(c_7\frac{\partial k}{\partial \xi}+c_8\frac{\partial k}{\partial \eta}+c_9\frac{\partial k}{\partial \zeta}\right)\\ \rho DW\varepsilon-\mu_\varepsilon\left(c_7\frac{\partial \varepsilon}{\partial \xi}+c_8\frac{\partial \varepsilon}{\partial \eta}+c_9\frac{\partial \varepsilon}{\partial \zeta}\right)\end{pmatrix}$$

and

$$\begin{aligned} s_1 &= D(\Theta-\rho\varepsilon) & \qquad \mu_k &= \mu_l+\mu_t/\sigma_k\\ s_2 &= D(t_1\Theta-t_2\rho\varepsilon)\varepsilon/k & \qquad \mu_\varepsilon &= \mu_l+\mu_t/\sigma_\varepsilon \end{aligned}$$

for which the production rate of the turbulence kinetic energy can be defined as

$$\begin{aligned}\Theta=&\left(2\mu_t\frac{\partial u}{\partial x}-\frac{2}{3}\left(\rho k+\mu_t\left(\frac{\partial u}{\partial x}+\frac{\partial v}{\partial y}+\frac{\partial w}{\partial z}\right)\right)\right)\frac{\partial u}{\partial x}+\left(2\mu_t\frac{\partial v}{\partial y}-\frac{2}{3}\left(\rho k+\mu_t\left(\frac{\partial u}{\partial x}+\frac{\partial v}{\partial y}+\frac{\partial w}{\partial z}\right)\right)\right)\frac{\partial v}{\partial y}\\ &+\left(2\mu_t\frac{\partial w}{\partial z}-\frac{2}{3}\left(\rho k+\mu_t\left(\frac{\partial u}{\partial x}+\frac{\partial v}{\partial y}+\frac{\partial w}{\partial z}\right)\right)\right)\frac{\partial w}{\partial z}+\mu_t\left(\frac{\partial u}{\partial y}+\frac{\partial u}{\partial z}+\frac{\partial v}{\partial x}+\frac{\partial v}{\partial z}+\frac{\partial w}{\partial x}+\frac{\partial w}{\partial y}\right)^2\end{aligned}$$

The standard Launder and Spalding[1] constants

$$C_\mu=0.09 \qquad t_1=1.44 \qquad t_2=1.92 \qquad \sigma_k=1.0 \qquad \sigma_\varepsilon=1.3$$

were used throughout this work and no attempt was made to model nonisotropic turbulence.

The transformed Navier-Stokes and $k-\varepsilon$ equations are discretized by a finite volume formulation that approximates the spatial differences as a net flux across the faces of each mesh cell.[3] Viscous stresses and geometric quantities are evaluated directly on the cell faces, while the flow and $k-\varepsilon$ variables are averaged over values found in adjacent cells. The unsteady equations are discretized into a linearized implicit delta form whose steady state solutions are not time-step dependent. To minimise the construction of the implicit operator, only the inviscid flux vectors are linearised. The flow equations can be written:

$$\left[I+\mu_i\Delta t(\delta_\xi A+\delta_\eta B+\delta_\zeta C)\right]\Delta\vec{W}^n_{ijk}=-\Delta t(\delta_\xi(\vec{F}-\vec{F}_v)+\delta_\eta(\vec{G}-\vec{G}_v)+\delta_\zeta(\vec{H}-\vec{H}_v))^n_{ijk} \tag{4}$$

where $\Delta\vec{W}^n=\vec{W}^{n+1}-\vec{W}^n$; Δt is the time step size; $0\le\mu_i\le 1$ is a parameter governing the degree of implicitness; δ and $\bar{\delta}$ are cell- and face-centered central differences; I is the identity matrix; and A, B, and C are the inviscid flux Jacobian matrices relative to the vectors $\vec{F}$, $\vec{G}$, and $\vec{H}$. An implicit form of the $k-\varepsilon$ equations can also be written:

$$\left[I+\mu_i\Delta t(\delta_\xi A_{k\varepsilon}+\delta_\eta B_{k\varepsilon}+\delta_\zeta C_{k\varepsilon}-E_{k\varepsilon})\right]\Delta\vec{W}^n_{k\varepsilon}|_{ijk}=-\Delta t(\bar{\delta}_\xi\vec{F}_{k\varepsilon}+\bar{\delta}_\eta\vec{G}_{k\varepsilon}+\bar{\delta}_\zeta\vec{H}_{k\varepsilon}-\vec{S}_{k\varepsilon})^n_{ijk} \tag{5}$$

where $A_{k\varepsilon}$, $B_{k\varepsilon}$, and $C_{k\varepsilon}$ are the inviscid flux Jacobian matrices relative to the inviscid terms found in the vectors $\vec{F}_{k\varepsilon}$, $\vec{G}_{k\varepsilon}$, and $\vec{H}_{k\varepsilon}$; and $E_{k\varepsilon}$ is the Jacobian matrix relative to the source vector $\vec{S}_{k\varepsilon}$.

Artificial Dissipation

Explicit artificial dissipation terms must be added to this centered finite volume formulation to suppress possible odd and even point oscillations and shock overshoots. Fourth difference terms, similar to those used by Jameson[4] and Pulliam,[5] are added throughout the flow field to prevent odd-even decoupling, while second difference terms are added near shocks to stabilize the flow calculation. A local Mach number scaling is used to reduce the artificial dissipation in viscous-dominated flow regions and is similar to the treatment suggested by Flores and Holst.[6] The local Mach number scaling is normalised by the inflow Mach number and limited to a maximum value of unity.

LU Approximate Factorization

The equations are solved by approximately factoring the block-banded implicit operator into two block triangular ones. The LU factorisation, which is based on one-sided spatial differences, can be written for the flow equations as:

$$\Big[I + \mu_i \Delta t(\delta_\xi^- A_1 + \delta_\eta^- B_1 + \delta_\varsigma^- C_1)\Big]\Big[I + \mu_i \Delta t(\delta_\xi^+ A_2 + \delta_\eta^+ B_2 + \delta_\varsigma^+ C_2)\Big]\Delta\vec{W}^n_{ijk} =$$
$$-\Delta t(\delta_\xi(\vec{F} - \vec{F}_v) + \delta_\eta(\vec{G} - \vec{G}_v) + \delta_\varsigma(\vec{H} - \vec{H}_v) + \vec{T})^n_{ijk} \tag{6}$$

and for the $k-\epsilon$ equations as follows:

$$\Big[I + \mu_i \Delta t(\delta_\xi^- A_{k\epsilon_1} + \delta_\eta^- B_{k\epsilon_1} + \delta_\varsigma^- C_{k\epsilon_1} - E_{k\epsilon_1})\Big]\Big[I + \mu_i \Delta t(\delta_\xi^+ A_{k\epsilon_2} + \delta_\eta^+ B_{k\epsilon_2} + \delta_\varsigma^+ C_{k\epsilon_2} - E_{k\epsilon_2})\Big]\Delta\vec{W}_{k\epsilon}|^n_{ijk}$$
$$= -\Delta t(\delta_\xi \vec{F}_{k\epsilon} + \delta_\eta \vec{G}_{k\epsilon} + \delta_\varsigma \vec{H}_{k\epsilon} + \vec{T}_{k\epsilon} - \vec{S}_{k\epsilon})^n_{ijk} \tag{7}$$

where δ^+ and δ^- are cell-centered forward and backward first differences; and $A_1 = 0.5(A + \beta|A|I)$ and $A_2 = 0.5(A - \beta|A|I)$ are the reconstructed flux Jacobian matrices, where $|A| = max(|\lambda_A|)$ is the maximum absolute-valued eigenvalue of the Jacobian matrix A. $\beta \approx 1$ is a scalar constant governing the amount of implicit dissipation produced by the matrix reconstructions, and I is the identity matrix. The vectors T and $T_{k\epsilon}$ represent the artificial dissipation terms added to the numerical schemes. These implicit systems of equations are solved by a two step procedure which, through back substitution, can be reduced to simple 5x5 matrix systems at every mesh cell. These reduced systems can be written for the flow equations:

1) Lower Sweep

$$\Big[I + \mu_i \Delta t(A_1 + B_1 + C_1)\Big]\Delta\vec{Y}^n_{ijk} = -\Delta t(\delta_\xi(\vec{F} - \vec{F}_v) + \delta_\eta(\vec{G} - \vec{G}_v) + \delta_\varsigma(\vec{H} - \vec{H}_v) + \vec{T})^n_{ijk}$$
$$+ \mu_i \Delta t(A_1 \Delta\vec{Y}^n_{i-1,j,k} + B_1 \Delta\vec{Y}^n_{i,j-1,k} + C_1 \Delta\vec{Y}^n_{i,j,k-1}) \tag{8}$$

2) Upper Sweep

$$\Big[I - \mu_i \Delta t(A_2 + B_2 + C_2)\Big]\Delta\vec{W}^n_{ijk} = \Delta\vec{Y}^n_{ijk} - \mu_i \Delta t(A_2 \Delta\vec{W}^n_{i+1,j,k} + B_2 \Delta\vec{W}^n_{i,j+1,k} + C_2 \Delta\vec{W}^n_{i,j,k+1}) \tag{9}$$

and for the $k-\epsilon$ equations

1) Lower Sweep

$$\Big[I + \mu_i \Delta t(A_{k\epsilon_1} + B_{k\epsilon_1} + C_{k\epsilon_1} - E_{k\epsilon_1})\Big]\Delta\vec{Y}_{k\epsilon}|^n_{ijk} = -\Delta t(\delta_\xi \vec{F}_{k\epsilon} + \delta_\eta \vec{G}_{k\epsilon} + \delta_\varsigma \vec{H}_{k\epsilon} - E_{k\epsilon} + \vec{T}_{k\epsilon})^n_{ijk}$$
$$+\mu_i \Delta t(A_{k\epsilon_1} \Delta\vec{Y}_{k\epsilon}|^n_{i-1,j,k} + B_{k\epsilon_1} \Delta\vec{Y}_{k\epsilon}|^n_{i,j-1,k} + C_{k\epsilon_1} \Delta\vec{Y}_{k\epsilon}|^n_{i,j,k-1}) \tag{10}$$

2) Upper Sweep

$$\left[I - \mu_i \Delta t(A_{k\varepsilon_2} + B_{k\varepsilon_2} + C_{k\varepsilon_2} - E_{k\varepsilon_2})\right] \Delta \vec{W}_{k\varepsilon}|^n_{ijk} = \Delta \vec{Y}_{k\varepsilon}|^n_{ijk} - \mu_i \Delta t(A_{k\varepsilon_2} \Delta \vec{W}_{k\varepsilon}|^n_{i+1,j,k} + B_{k\varepsilon_2} \Delta \vec{W}_{k\varepsilon}|^n_{i,j+1,k} + C_{k\varepsilon_2} \Delta \vec{W}_{k\varepsilon}|^n_{i,j,k+1}) \tag{11}$$

Diagonally Inverted LU Factorization

The $k-\varepsilon$ equations are solved algebraically, while the flow equations are diagonally inverted using the similarity transformation:[1]

$$Q^{-1}(A+B+C)Q = \Lambda$$

where

$$\lambda_{11} = \lambda_{22} = \lambda_{33} = U + V + W$$
$$\lambda_{44} = U + V + W - c\sqrt{l_1^2 + l_2^2 + l_3^2}$$
$$\lambda_{55} = U + V + W + c\sqrt{l_1^2 + l_2^2 + l_3^2}$$
$$\lambda_{ij} = 0 \qquad when \qquad i \neq j$$

$$q^2 = u^2 + v^2 + w^2 \qquad l_2 = \xi_y + \eta_y + \varsigma_y$$
$$l_1 = \xi_x + \eta_x + \varsigma_x \qquad l_3 = \xi_z + \eta_z + \varsigma_z$$

and c is the local speed of sound. For a local time step defined as:

$$\Delta t = \frac{Cn}{(|A| + |B| + |C|)}$$

where Cn is the Courant number, the lower and upper sweeps, Eqs. 8 and 9, can be approximated by the following scalar equations($m = 1, ..., 5$).

1) Lower Sweep

$$(Q^{-1}\Delta \vec{Y}^n_{ijk})_m = \frac{\begin{pmatrix} -\Delta t\Big(Q^{-1}(\delta_\xi(\vec{F} - \vec{F}_v) + \delta_\eta(\vec{G} - \vec{G}_v) + \delta_\varsigma(\vec{H} - \vec{H}_v) + \vec{T})^n_{ijk} \\ -\mu_i(\tilde{D}_{a_1} Q^{-1} \Delta \vec{Y}^n_{i-1,j,k} + \tilde{D}_{b_1} Q^{-1} \Delta \vec{Y}^n_{i,j-1,k} \\ +\tilde{D}_{c_1} Q^{-1} \Delta \vec{Y}^n_{i,j,k-1})\Big) \end{pmatrix}_m}{\Big((1 + \mu_i \beta Cn/2)I + \mu \Delta t \Lambda/2\Big)_m} \tag{12}$$

2) Upper Sweep

$$(Q^{-1}\Delta \vec{W}^n_{ijk})_m = \frac{\begin{pmatrix} Q^{-1}\Delta \vec{Y}^n_{ijk} - \mu_i \Delta t(\tilde{D}_{a_2} Q^{-1} \Delta \vec{W}^n_{i+1,j,k} \\ +\tilde{D}_{b_2} Q^{-1} \Delta \vec{W}^n_{i,j+1,k} + \tilde{D}_{c_2} Q^{-1} \Delta \vec{W}^n_{i,j,k+1}) \end{pmatrix}_m}{\Big((1 + \mu_i \beta Cn/2)I - \mu \Delta t \Lambda/2\Big)_m} \tag{13}$$

where $\tilde{D}_{a_1} = 0.5(\tilde{D}_a + \beta|A|I)$; $\tilde{D}_{a_2} = 0.5(\tilde{D}_a - \beta|A|I)$; and $\tilde{D}_a$ contains only the diagonal elements of the symmetric matrix $Q^{-1}AQ$ [i.e., $\tilde{d}_{a_{11}} = \tilde{d}_{a_{22}} = \tilde{d}_{a_{33}} = U$; $\tilde{d}_{a_{44}} = U + c(\xi_x l_1 + \xi_y l_2 + \xi_z l_3)$; and $\tilde{d}_{a_{55}} = U - c(\xi_x l_1 + \xi_y l_2 + \xi_z l_3)$, with similar terms for $\tilde{D}_{b_1}$, $\tilde{D}_{b_2}$, $\tilde{D}_{c_1}$, and $\tilde{D}_{c_2}$)].

Initial and Boundary Conditions

A uniform flow field based on an initial guess of the upstream conditions is used to start both the flow and $k-\varepsilon$ calculations. A no-slip condition is enforced along the solid boundaries and thus only pressures need

to be specified along the solid walls. These pressures are obtained from a three-dimensional interpretation of the normal momentum analysis developed by Rissi.[7]

Total pressure, total temperature, and two flow angles are specified at subsonic inflow boundaries, while a one-dimensional Rieman invariant is extrapolated from the interior flow field. An inlet total temperature is fixed while a power law velocity profile is specified by varying the inlet total pressure. This treatment attempts to simulate an incoming boundary-layer profile.[8] The specified condition at a subsonic outflow boundary is a nonreflective treatment that attempts to minimise unwanted reflected waves.[9] Static pressures are obtained from a radial momentum analysis and then coupled with the incoming compatibility relation to produce a nonreflective boundary condition.

An assumed two percent upstream turbulence intensity is used as an inflow boundary condition while the specified condition at the outflow boundary is a zeroth order extrapolation of the k and ε variables.

Turbulent viscosities are set to zero along solid walls while a wall function[2] is used to evaluate the $k-\varepsilon$ variables in cells immediately adjacent to these solid boundaries.

Steady State Calculations

Local time-stepping and the multigrid method are used to accelerate the convergence of steady state calculations.

A locally varying time step size, based on a constant Courant number, is defined throughout the flow field. This preconditioning creates a warped time integration that can accelerate calculations to a steady state without affecting the final solution. Local time stepping is used for both the flow and $k-\varepsilon$ equations, although the value of the Courant numbers used in their integration may vary.

The flow algorithm is developed within the framework of the multigrid method to increase the efficiency of the time-marching procedure. Following the work of Jameson,[10] the basic flow algorithm is used to resolve the high frequency errors present on any current grid level (h), while the multigrid method is used to eliminate the lower frequencies through a sequence of calculations on coarser grids ($2h, 4h, 8h, \ldots$). A four-level W-cycle, where a single flow calculation is performed on each grid level before transfering information to their respective coarser grids, was found to be the most efficient means of accelerating the steady state calculations. Coarse grid boundary conditions are identical to those on the fine grid, with the exception being that inflow/outflow conditions are updated only on the finest grid. The viscous fluxes are evaluated only on the finest grid, and thus influence the coarser grid calculations only through the transfered fine grid residual.

The $k-\varepsilon$ equations are solved every multigrid cycle but only on the finest grid. They are not accelerated by the multigrid method defined above, which requires approximately 1.32 work units of computational effort. (One work unit is equivalent to a single Navier-Stokes calculation on the finest grid.) There is little to be gained by multigridding the $k-\varepsilon$ equations between each fine grid flow solution since it is the time asymptote, rather than the solution at any current time level, that is ultimately required. Moreover, a coarse grid wall function, consistent with the fine grid flow field, is not easily defined and thus prohibits the simultaneous multigridding of both the flow and $k-\varepsilon$ equations. In addition, the viscous stresses cannot be adequately resolved on the coarser grids and thus their neglect at worst creates a high frequency error that, in any event, cannot be sustained by the multigrid method.

Vector Sequence Acceleration Methods

A number of vector sequence extrapolation methods have been used to accelerate steady state flow calculations.[11,12,13] Most of these methods assume a slowly converging asymptotic linear behavior of the form

$$W^{n+1} = AW^n + b \tag{14}$$

where W is the flow solution, b is an arbitrary vector, and A is the iteration matrix, whose largest eigenvalue has a magnitude close to unity. To remove the influence of the largest eigenvalue(s), and thus increase the rate of convergence, a number of extrapolation methods have been developed.[14] One such method is Eddy's[15] and Mesina's[16] Reduced Rank Extrapolation. This method can be described as follows:

Given the vector sequence $W^{n+k-1}, W^{n+k-2}, \ldots, W^n$; where $k \leq n$, the following difference terms can be constructed

$$R^n = W^{n+1} - W^n$$

$$\widehat{R^n} = R^{n+1} - R^n$$

such that the solution of the normalised system of equations

$$\sum_{j=0}^{k-1} (\widehat{R^{n+i}}, \widehat{R^{n+j}}) c_j = -(\widehat{R^{n+i}}, R^n) \qquad i = 0, 1..., k-1 \tag{15}$$

(where $(\widehat{R^{n+i}}, \widehat{R^{n+j}})$ is the inner product of the two vectors, $\widehat{R^{n+i}}$ and $\widehat{R^{n+j}}$), can be used to construct an extrapolated solution:

$$W_{ex} = \sum_{j=0}^{k} \gamma_j W^{n+j} \tag{16}$$

where

$$\gamma_0 = 1 - c_0$$
$$\gamma_j = c_{j-1} - c_j \qquad 1 \leq j \leq k-1$$
$$\gamma_k = c_{k-1}$$

For a fixed value of k, the accuracy of this extrapolated solution increases as n increases. In general it is true that the greatest amount of acceleration is produced when only a small value of k is needed to influence a small number of eigenvalues with large moduli. If a large number of dominant eigenvalues are of similar magnitude, then the extrapolation method may be of limited value since the manipulation of an equally large number of vectors would be required. As k increases, the solution of Eq. 15 becomes more sensitive to truncation errors and thus the accuracy of the extrapolated solution decreases.

These vector sequence methods can also be used to analyse the convergence properties of any iterative method.[17] It can be shown[18] that, for n sufficiently large, the zeros of the polynomial

$$\sum_{j=0}^{k} \gamma_j \lambda^j = 0 \tag{17}$$

are estimates of the k largest eigenvalues of the iteration matrix A. Even though these values are only approximates, their locations with respect to one another can be used to analyse the convergence properties of the iterative method and predict the effectiveness of a vector sequence extrapolation.

Results

Numerical results for the flow through an annular turbine are used to illustrate this diagonally inverted LU implicit multigrid scheme's ability to calculate three-dimensional compressible viscous flows.

Turbomachinery calculations were performed on H-type grids consisting of 96x24x24 mesh cells in the throughflow, blade-to-blade, and radial directions, respectively. All calculations were performed on the NASA-Lewis CRAY X-MP, where approximately 1.5 million words of memory and 40 minutes of CPU time were required for a calculation consisting of 211 work units.

The annular turbine, designed and tested at NASA Lewis,[19,20] is shown in Figure 1. This blade row is made up of 36 core turbine stator vanes, 38.10 mm high, with an axial chord of 38.23 mm. The stator has a tip diameter of 508 mm and a 0.85 hub-to-tip radius ratio. Mesh cells found immediately adjacent to solid walls are centered at distances 0.002 of an axial chord away, which correspond to a value of $60 \leq Y^+ \leq 200$ for the following flow calculations.

Experimental test conditions of ambient axial inflow and a 0.65 hub-static to inlet-total pressure ratio produce a flow field with mean radius inlet and exit critical velocity ratios of 0.231 and 0.778, respectively. To match the upstream flow conditions (an inflow Mach number of 0.211), these nonrotating calculations were run with a 0.665 hub-static to inlet-total pressure ratio.

The resulting flow field is fully subsonic and is compared with experimental data at three spanwise positions. Figures 2, 3, and 4 compare the calculated blade surface static pressure distributions (normalised by inlet total pressure) at 13.3, 50, and 86.7 percent span with the experimental data produced by Goldman and Seasholtz.[19] Due to the bluntness of the blade's trailing edge, the flow in this region is not sufficiently resolved, but the overall pressure distributions agree well with the experimental data. The calculations are most significant near the uncovered portion of the blade's suction surface, where an inadequate turbulence model can greatly affect the accuracy of the flow solution.

Figure 5 shows the critical velocity ratio distributions along the 9, 50, and 81.7 percent radial span planes at the 155.8 percent axial chord location. The agreement between the computational and experimental results is extremely good and increases as one moves away from the hub and towards the tip region. The differences near the hub may be due to secondary flow and the non-isotropic turbulence found within this region. In general, the flow calculation has captured the viscous wake effects and agrees well with the experimental data. These results are obtained with the $k-\varepsilon$ turbulence model, which unlike the more widely used algebraic models, does not require the implimentation of an explicit wake model.

Figure 6 shows the flow angles at the previously defined grid locations. The computational results compare extremely well with the experimental data at mid-span but deviate from the experimental data as one moves towards the hub and tip regions. These results are due to the underprediction of the boundary layer thicknesses and are not unexpected since the $k-\varepsilon$ model assumes fully turbulent flow and a transition model has not been incorporated into the calculation.

Overall the numerical calculations compare extremely well with the experimental data and demonstrate the scheme's ability to calculate three-dimensional viscous flows.

To investigate the convergence properties of this multigrid scheme, a number of flow calculations, both viscous and inviscid, were performed. In all cases a Courant number of six was used to solve the flow equations while a Courant number of four was used for the $k-\varepsilon$ equations. The inviscid solutions were calculated on a 64x16x16 grid, which was of a relative fineness, comparable to that used for the viscous calculations. This was done in an attempt to insure that each of the flow calculations was performed on computational grids relevant to their respective length scales. It would seem to make little sense to perform viscous calculations on inviscid grids and vice versa. Thus, in order for meaningful comparisons to be made, each calculation, both viscous and inviscid, was performed on grids whose sizes were relevant to the physical problems being addressed.

After four hundred work units on a single grid, the viscous flow calculation's convergence history (Figure 7) shows that the residual of the continuity equation has been reduced only two and a half orders of magnitude. An abrupt 'flattening out' of the convergence history occurs after 300 work units and thus any further reduction would require significantly more iterations. The corresponding eigenvalue plot for this calculation is shown in Figure 8, where twenty-two of the largest eigenvalues are plotted in the complex plane. All of the eigenvalues have relatively equal magnitude and are thus located on a circle centered at the origin. This type of structure is characteristic of optimized SOR schemes,[21] which are analogous to the LU implicit method in that both techniques require a back substitution step. Because of the large number of dominant eigenvalues, a vector sequence extrapolation would, in all likelihood, prove to be ineffective. The presence of virtually all of the eigenvalues would have to be accounted for before any amount of acceleration could be produced.

The multigrid method is another way to accelerate convergence. Figure 9 shows the convergence history of the viscous multigrid calculation where a residual drop of approximately four and a half orders of magnitude was produced within 400 work units. The convergence acceleration is produced by a reduction in the magnitude of the largest eigenvalue(s), which are most likely associated with a low or intermediate spatial frequency. It is also interesting to discover that the multigrid method has altered the basic eigenvalue structure. The structure of the multigrid calculation, Figure 10, is clearly less clustered than that of the single grid solution. These results suggest that a multigrid scheme is more likely to benefit from a vector sequence extrapolation, an observation that has been confirmed in practice, by Reddy and Jacocks.[22]

These trends are also observed in the inviscid calculations. The convergence history (Figure 11) and eigenvalue structure (Figure 12) of the inviscid, single grid calculation again suggest the unlikelihood of using a vector sequence extrapolation method to accelerate convergence. The multigrid method produces a significant amount of convergence acceleration (Figure 13) and again has a less clustered eigenvalue structure (Figure 14). These calculations are more likely to be accelerated by a vector sequence extrapolation. Since both the inviscid and viscous eigenvalue plots are similar in structure (at least for the largest values), it would seem that, either inherently or by design, the convergence properties of the iterative procedures are inviscidly dominated (inviscid in the sense that the high frequency modes most often associated with viscous effects do not seem to be dominating the convergence rates). This speculation is not unreasonable since it is also true that the viscous fluxes were not included in the implicit operator of the LU scheme. The differences in the amount of convergence acceleration produced by the viscous and inviscid multigrid calculations may be attributed more to differences in grid size and stretching, and less to viscous effects.

Eriksson and Rizzi[23] found that the most persistant eigenmodes in their inviscid Runga-Kutta calculations were most often associated with high spatial frequencies. They speculated that these high frequency modes could not be removed by the multigrid method, which operates on low frequency errors. Others have suggested that there would be little opportunity to accelerate viscous calculations since they presumably contain even more high frequency modes then do the inviscid equations. However, the existence of a number of successful multigrid calculations indicates that there are significant amounts of low or intermediate

frequencies governing the convergence rates of a number of single grid calculations. The convergence acceleration and modified eigenvalue structure produced by the multigrid method are evidence that a number of low frequency modes are dominant in these single grid calculations (Figures 7,8,11, and 12) and that they can be removed by the multigrid method (Figures 9,10,13 and 14). This analysis could also explain why a significant amount of acceleration occurs in the viscous calculations since presumably these low frequency modes exist in both the Euler and Navier-Stokes equations.

In any event, the large number of dominant eigenvalues would prohibit the effectiveness of a vector sequence extrapolation in either the single or multigrid calculations. The eigenvalue plots suggest that at least 25-30 eigenvalues would have to be accounted for before any significant amount of acceleration could be achieved. This prediction is confirmed in Figure 15, where only a slight amount of acceleration (12 percent more than the base multigrid convergence rate shown in Figure 9) is produced by the storage and manipulation of 25 viscous multigrid flow solutions. Although these results may seem discouraging, vector sequence methods are highly problem dependent and may be of greater value in other flow calculations. In addition, the eigenvalue estimates are extremely useful in the analysis of any iterative method.

Concluding Remarks

The convergence properties of an implicit multigrid scheme have been investigated for the calculation of complex three-dimensional flows. A vector extrapolation method was used to calculate eigenvalue estimates of the iterative procedure to gain a further understanding of the process by which the multigrid method accelerates calculations to steady state.

Results illustrate both the scheme's ability to calculate turbulent viscous flows and the convergence acceleration produced by the multigrid method.

Acknowledgements

It is with pleasure that I acknowledge a number of conversations on vector extrapolation methods held with Dr. Avram Sidi. I would also like to acknowledge the assistance offered throughout the course of this work by Dr. Kristine Dugas.

References

[1] Yokota, J.W., Caughey, D.A., and Chima, R.V., "A Diagonally Inverted LU Implicit Multigrid Scheme," *Proceedings of the First National Fluid Dynamics Congress*, Part 1, pp. 104-111, AIAA Press, Cincinnati, Ohio, July 1988.

[2] Launder, B.E., and Spalding, D.B., "The Numerical Computation of Turbulent Flows," *Computer Methods in Applied Mechanics and Engineering*, vol. 3, pp. 269-289, 1974.

[3] Yokota, J.W., "A Diagonally Inverted LU Implicit Multigrid Scheme for the 3-D Navier-Stokes Equations and a Two Equation Model of Turbulence," AIAA Paper 89-0467, 27th Aerospace Sciences Meeting, Reno, Nevada, January 1989.

[4] Jameson, A., "Transonic Flow Calculations for Aircraft," in *Lecture Notes in Mathematics*, Brezzi, F., ed., vol. 1127, pp. 156-242, Springer-Verlag, New York, 1985.

[5] Pulliam, T.H., "Artificial Dissipation Models for the Euler Equations," AIAA Paper 85-0438 , 23rd Aerospace Sciences Meeting, Reno, Nevada, January 1985.

[6] Flores, J., and Holst, T.L., "Numerical Solution of the Navier-Stokes Equations for Complex Configurations," *CFD for Aerospace Problems: Methods and Codes*, University of Tennessee Space Institute Workshop, UTSI Publication No. E02-4005 013-88, Reddy, K.C., and Steinhoff, J., ed., March 1988.

[7] Rizzi, A., "Numerical Implimentation of the Solid Body Boundary Conditions for the Euler Equations," ZAMM, vol. 58, pp. 301-304, 1978.

[8] Chima, R.V., and Yokota, J.W., "Numerical Analysis of Three-Dimensional Viscous Internal Flows," *Proceedings of the First National Fluid Dynamics Congress*, Part 1, pp. 17-24, AIAA Press, Cincinnati, Ohio, July 1988.

[9] Yokota, J.W., and Caughey, D.A., "An LU Implicit Multigrid Algorithm for the Three-Dimensional Euler Equations," *AIAA Journal* , Vol. 26, No. 9, pp. 1061-1069, September 1988.

[10] Jameson, A., "Solution of the Euler Equations for Two-Dimensional Transonic flows by a Multigrid Method," MAE Report 1613, Princeton University, 1983.

[11] Caughey, D.A., and Jameson, A., "Accelerated Iterative Calculation of Transonic Nacelle Flowfields," *AIAA Journal* , Vol. 15, No. 10, pp. 1474-1480, October 1977.

[12] Wigton, L.B., Yu, N.J., and Young, D.P., "GMRES Acceleration of Computational Fluid Dynamics Codes," AIAA Paper 85-1494, AIAA 7th Computational Fluid Dynamics Conference, Cincinnati, Ohio, 1985.

[13] Hafez, M., Parlette, E., and Salas, M., "Convergence acceleration of iterative solutions of Euler equations for transonic flow computations," *Computational Mechanics* , Vol. 1, pp. 165-176, 1986.

[14] Sidi, A., Ford, W.F., and Smith, D.A., "Acceleration of Convergence of Vector Sequences," *SIAM Journal of Numerical Analysis*, Vol. 23, No. 1, pp. 178-196, February 1986.

[15] Eddy, R.P., "Extrapolating to the limit of a Vector Sequence," *Information Linkage Between Applied Mathematics and Industry*, ed. P.C.C. Wang, Academic Press, pp. 387-396, 1979.

[16] Mesina, M., "Convergence Acceleration for the Iterative Solution of the Equation X = AX + F," *Computational Methods in Applied Mechanical Engineering*, Vol. 10, pp. 165-173, 1977.

[17] Cheer, A.Y., Saleem, M., Pulliam, T.H., and Hafez, M., "Analysis of the Convergence History of Flow through Nozzles with Shocks," *Proceedings of the First National Fluid Dynamics Congress*, Part 1, pp. 620-629, AIAA Press, Cincinnati, Ohio, July 1988.

[18] Sidi, A., and Bridger, J., "Convergence and stability analyses for some vector extrapolation methods in the presence of defective iterative matrices," *Journal of Computational Applied Mathematics*, vol. 22, pp. 35-61, 1988.

[19] Goldman, L.J., and McLallin, K.L., "Cold-Air Annular Cascade Investigation of Aerodynamic Performance of Core-Engine-Cooled Turbine Vanes. I: Solid-Vane Performance and Facility Description," NASA TM X-3224, 1975.

[20] Goldman, L.J., and Seasholtz, R.G., "Laser Anemometer Measurements in a Annular Cascade of Core Turbine Vanes and Comparison with Theory," NASA TP-2018, 1982.

[21] Sidi, A., Private Communication, July 1989.

[22] Reddy, K.C., and Jacocks, J.L., "A Locally Implict Scheme for the Euler Equations," AIAA Paper 87-1144, AIAA 8th Computational Fluid Dynamics Conference, Honolulu, Hawaii, 1987.

[23] Eriksson, L.E., and Rizzi, A., "Computer-Aided Analysis of the Convergence to Steady State of Discrete Approximations to the Euler Equations," *Journal of Computational Physics*, vol. 57, pp. 90-128, 1985.

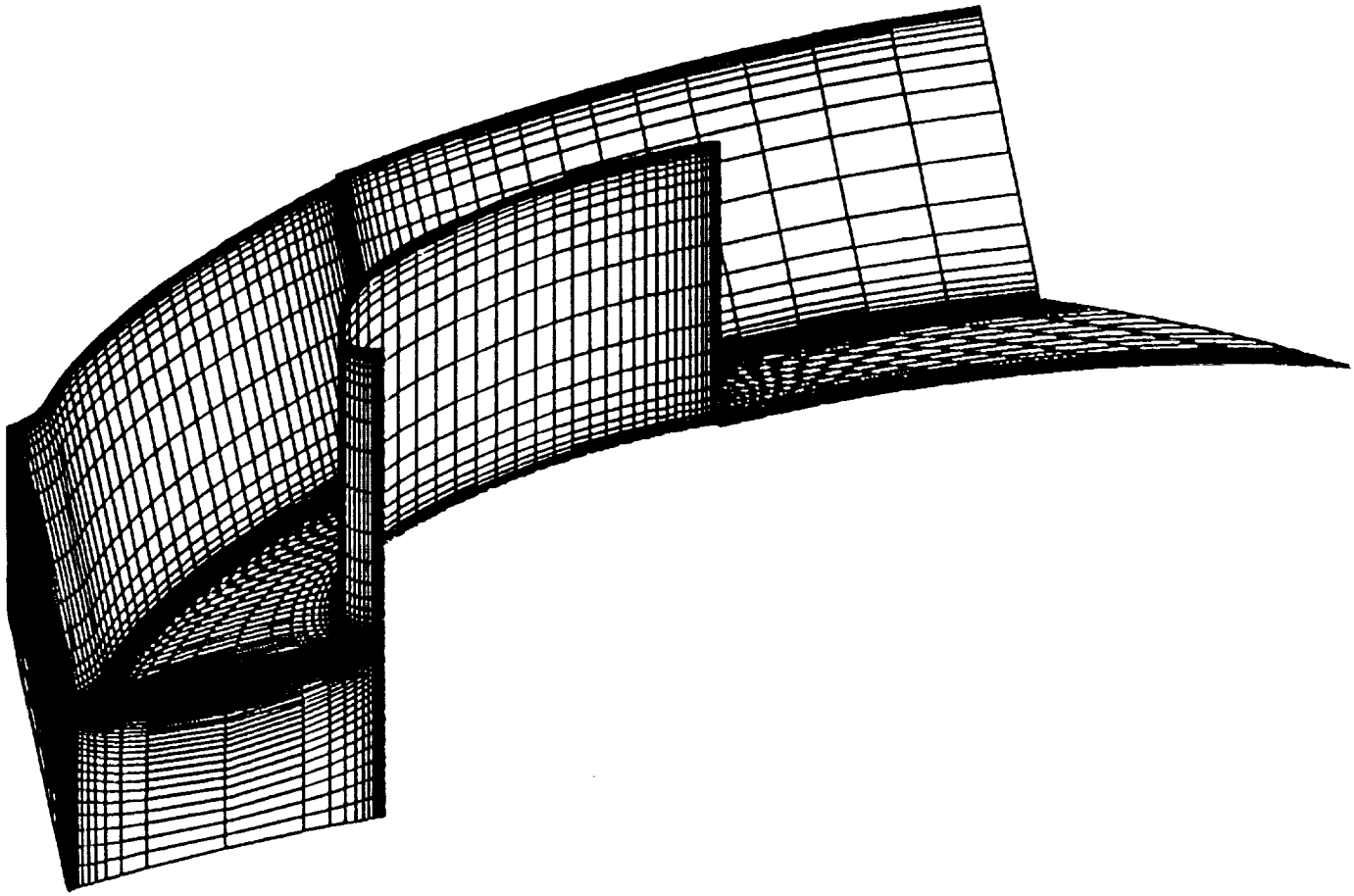

FIGURE 1. - COMPUTATIONAL GRID FOR THE ANNULAR CASCADE.

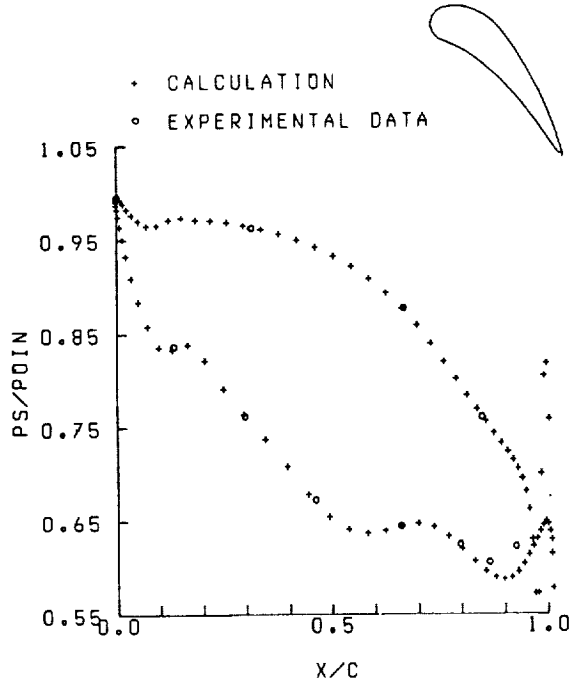

FIGURE 2. - STATIC PRESSURE BLADE DISTRIBUTION AT 13.3 PERCENT SPAN.

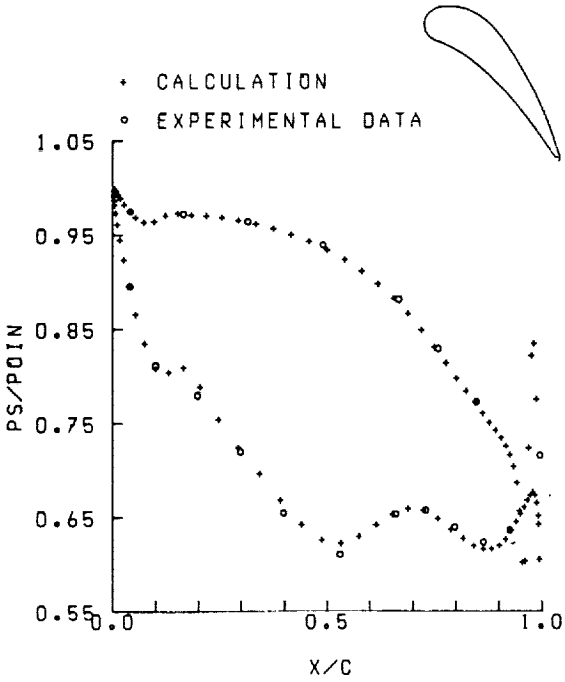

FIGURE 3. - STATIC PRESSURE BLADE DISTRIBUTION AT 50 PERCENT SPAN.

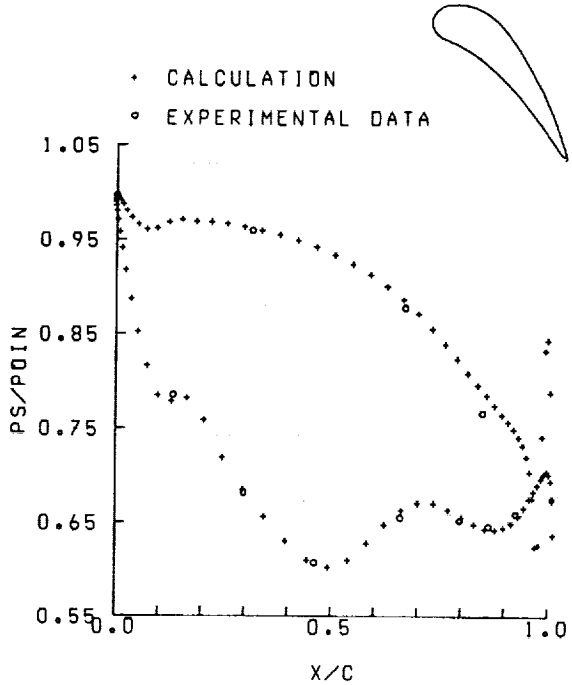

FIGURE 4. - STATIC PRESSURE BLADE DISTRIBUTION AT 86.7 PERCENT SPAN.

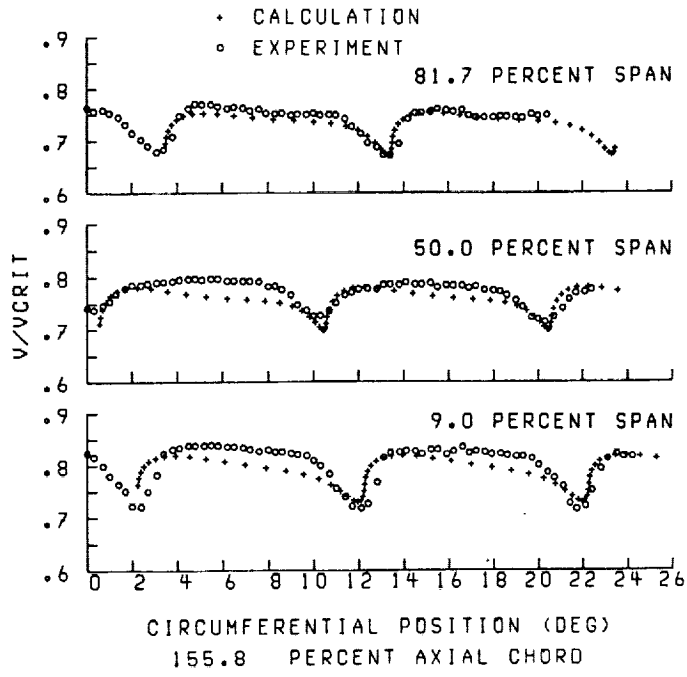

FIGURE 5. - CRITICAL VELOCITY RATIO AT 9, 50, AND 82 PERCENT SPAN AND 156 PERCENT AXIAL CHORD.

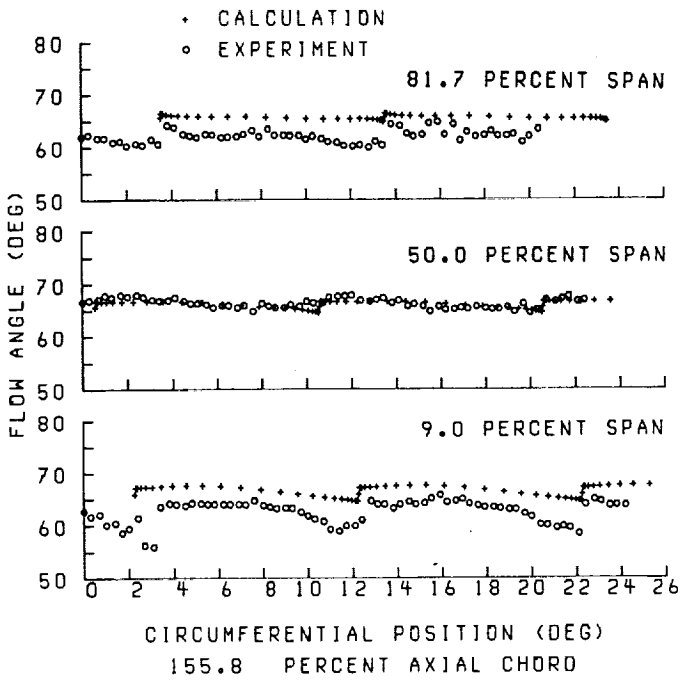

FIGURE 6. - FLOW ANGLE AT 9, 50, AND 82 PERCENT SPAN AND 156 PERCENT AXIAL CHORD.

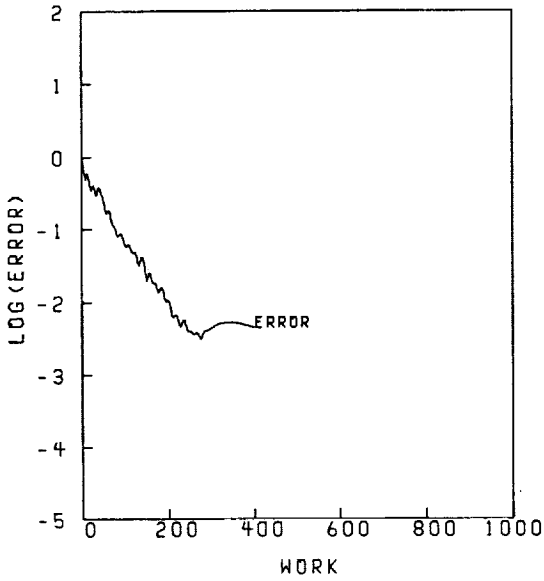

P.R. 0.6650 ANGY 90.00
ROT. 0.000 ANGZ 0.00
RES1 0.169E 01 RES2 0.760E-02
WORK 400.00 C.N. 6.0 RATE 0.9866

FIGURE 7. - CONVERGENCE HISTORY OF THE VISCOUS SINGLE GRID CALCULATION.

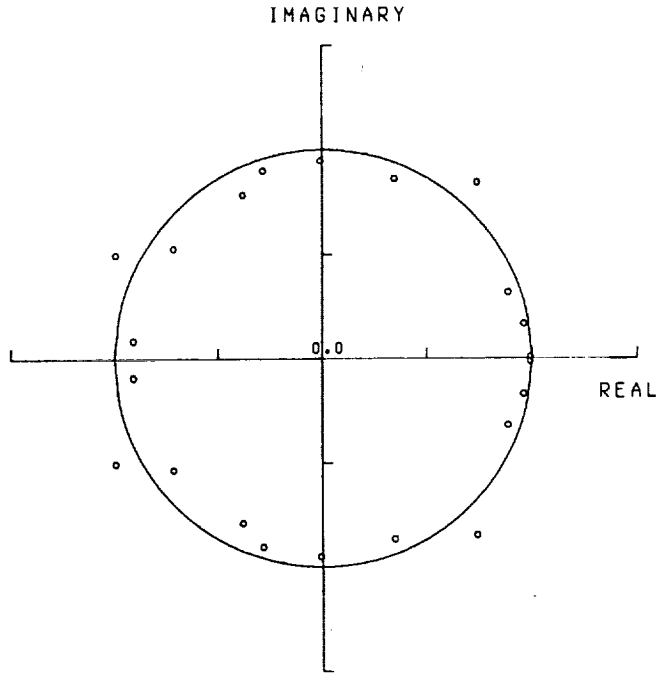

22.0 EIGENVALUES

FIGURE 8. - EIGENVALUE STRUCTURE OF THE VISCOUS SINGLE GRID CALCULATION.

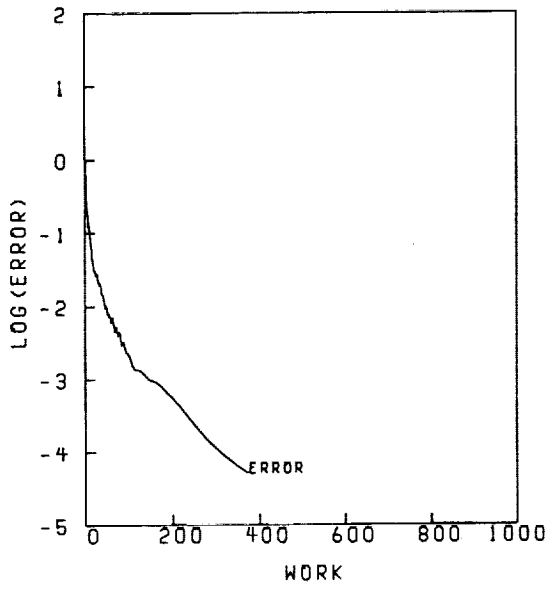

P.R. 0.6650 ANGY 90.00
ROT. 0.000 ANGZ 0.00
RES1 0.169E 01 RES2 0.871E-04
WORK 373.07 C.N. 6.0 RATE 0.9739

FIGURE 9. - CONVERGENCE HISTORY OF THE VISCOUS MULTIGRID CALCULATION.

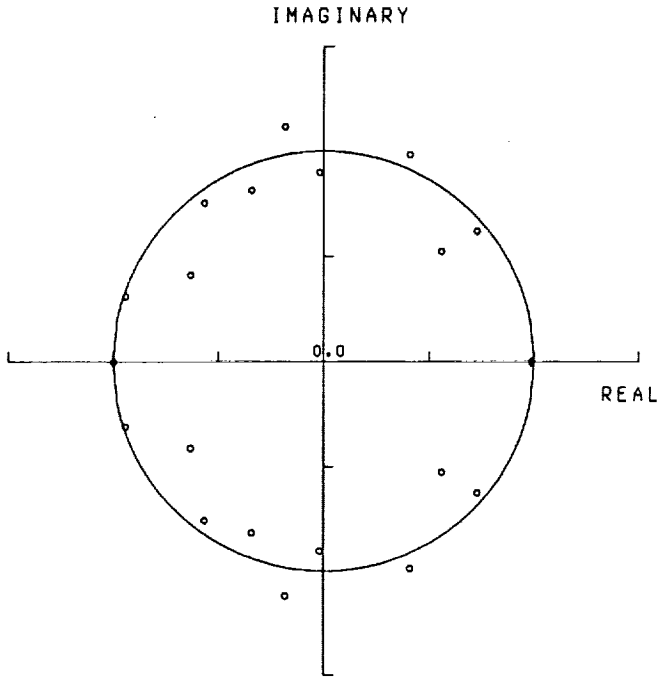

22.0 EIGENVALUES

FIGURE 10. - EIGENVALUE STRUCTURE OF THE VISCOUS MULTIGRID CALCULATION.

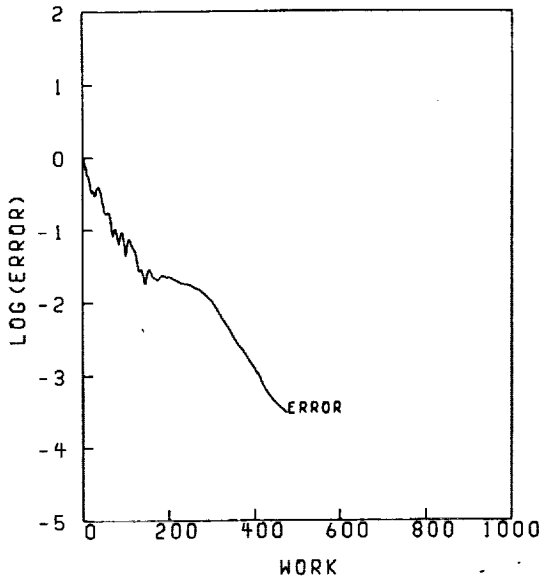

P.R. 0.6650 ANGY 90.00
ROT. 0.000 ANGZ 0.00
RES1 0.113E 01 RES2 0.343E-03
WORK 475.00 C.N. 6.0 RATE 0.9831

FIGURE 11. - CONVERGENCE HISTORY OF THE INVISCID SINGLE GRID CALCULATION.

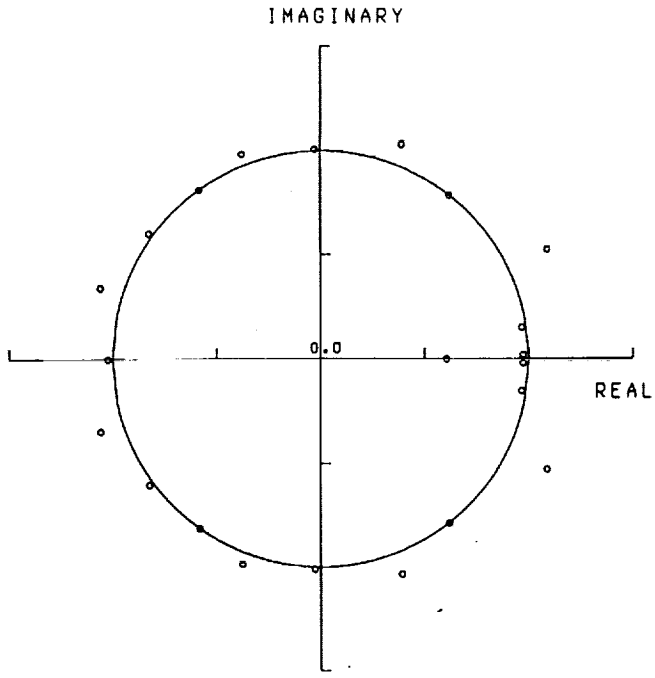

25.0 EIGENVALUES

FIGURE 12. - EIGENVALUE STRUCTURE OF THE INVISCID SINGLE GRID CALCULATION.

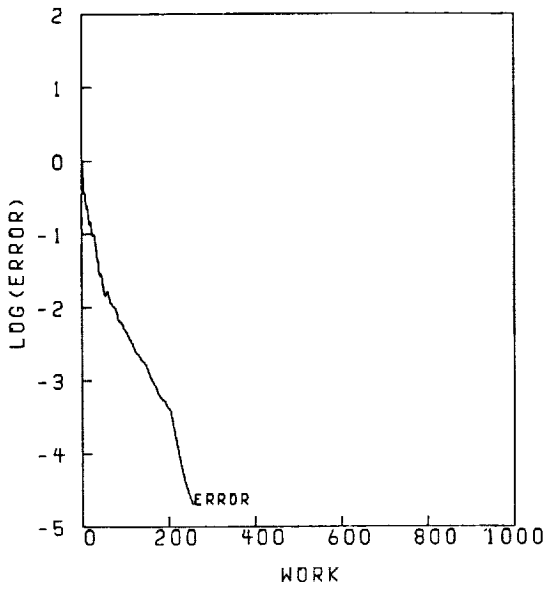

P.R. 0.6650 ANGY 90.00
ROT. 0.000 ANGZ 0.00
RES1 0.113E 01 RES2 0.229E-04
WORK 257.25 C.N. 6.0 RATE 0.9588

FIGURE 13. - CONVERGENCE HISTORY OF THE INVISCID MULTIGRID CALUCLATION.

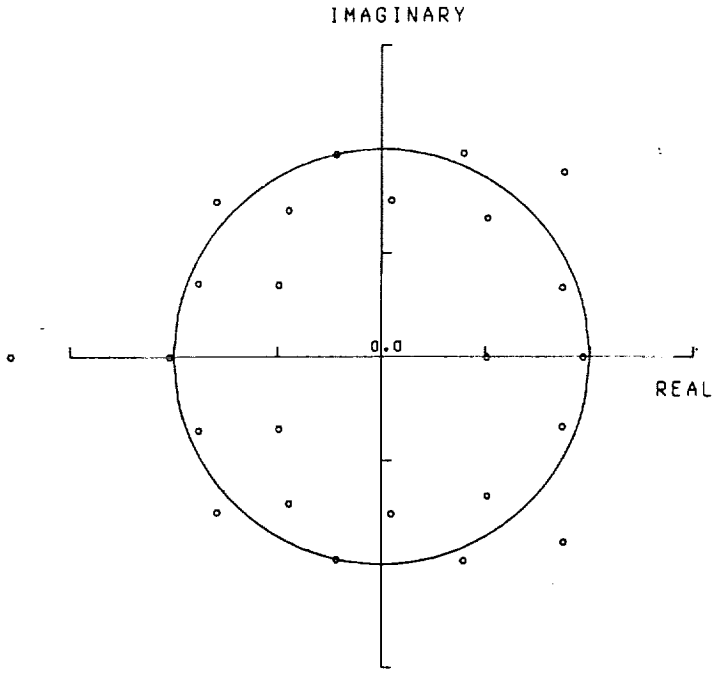

25.0 EIGENVALUES

FIGURE 14. - EIGENVALUE STRUCTURE OF THE INVISCID MULTIGRID CALCULATION.

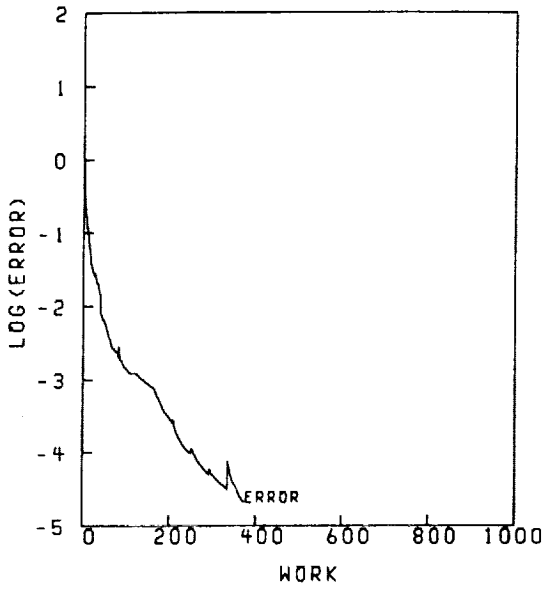

P.R. 0.6650 ANGY 90.00
ROT. 0.000 ANGZ 0.00
RES1 0.169E 01 RES2 0.358E-04
WORK 373.07 C.N. 6.0 RATE 0.9716

FIGURE 15. - CONVERGENCE HISTORY OF THE VECTOR SEQUENCE EXTRAPOLATED. VISCOUS MULTIGRID CALCULATION.

NASA
National Aeronautics and Space Administration

Report Documentation Page

1. Report No.	2. Government Accession No.	3. Recipient's Catalog No.
NASA CR-185154		

4. Title and Subtitle	5. Report Date
Multigrid Calculations of 3-D Turbulent Viscous Flows	October 1989
	6. Performing Organization Code

7. Author(s)	8. Performing Organization Report No.
Jeffrey W. Yokota	None (E-5116)
	10. Work Unit No.
	505-62-21

9. Performing Organization Name and Address	11. Contract or Grant No.
Sverdrup Technology, Inc. NASA Lewis Research Center Group Cleveland, Ohio 44135	NAS3-25266
	13. Type of Report and Period Covered Contractor Report Final
12. Sponsoring Agency Name and Address	14. Sponsoring Agency Code
National Aeronautics and Space Administration Lewis Research Center Cleveland, Ohio 44135-3191	

15. Supplementary Notes

Project Manager, John J. Adamczyk, Office of the Chief Scientist, NASA Lewis Research Center. Prepared for the First Canadian Symposium on Aerodynamics sponsored by the Canadian Aeronautics and Space Institute, Ottawa, Ontario, December 4-5, 1989.

16. Abstract

Convergence properties of a multigrid algorithm, developed to calculate compressible viscous flows, are analyzed by a vector sequence eigenvalue estimate. The full three-dimensional Reynolds-averaged Navier-Stokes equations are integrated by an implicit multigrid scheme while a $k-\epsilon$ turbulence model is solved, uncoupled from the flow equations. Estimates of the eigenvalue structure for both single and multigrid calculations are compared in an attempt to analyze the process as well as the results of the multigrid technique. The flow through an annular turbine is used to illustrate the scheme's ability to calculate complex three-dimensional flows.

17. Key Words (Suggested by Author(s))	18. Distribution Statement
Multigrid Turbulence Navier-Stokes	Unclassified – Unlimited Subject Category 01

19. Security Classif. (of this report)	20. Security Classif. (of this page)	21. No of pages	22. Price*
Unclassified	Unclassified		

*For sale by the National Technical Information Service, Springfield, Virginia 22161